PAPER

Controllable ALD synthesis of platinum nanoparticles by tuning different synthesis parameters

To cite this article: Chuandao Wang *et al* 2017 *J. Phys. D: Appl. Phys.* **50** 415301

View the article online for updates and enhancements.

Controllable ALD synthesis of platinum nanoparticles by tuning different synthesis parameters

Chuandao Wang[1,2,4]**, Linhua Hu**[2]**, Yuyuan Lin**[1,2]**, Kenneth Poeppelmeier**[2]**, Peter Stair**[2,3] **and Laurence Marks**[1]

[1] Department of Materials Science and Engineering, Northwestern University, 2220 North Campus Drive, Evanston, IL 60208-3108, United States of America
[2] Department of Chemistry, Northwestern University, 2145 Sheridan Road, Evanston, IL 60208-3113, United States of America
[3] Chemical Sciences and Engineering Division, Argonne National Laboratory, 9700 South Cass Avenue, Argonne, IL 60439, United States of America

E-mail: ericenkin@gmail.com

CrossMark

Abstract

Pt nanoparticles were successfully deposited using three different atomic layer deposition (ALD) methods, e.g. AB-type, ABC-type and static ABC-type ALD, on two different types of strontium titanate nanocuboids (STO-NCs) samples in a reaction temperature window of 125 °C–300 °C. The influence of reaction temperature, number of ALD cycles, type of substrate, 2nd reagent and type of ALD method on Pt nanoparticle deposition are comprehensively studied and discussed in this work. Varying the reaction temperature and number of cycles across the three different ALD methods affects Pt particle size, density, and loading. Surface termination of STO-NCs substrate will change deposited Pt nanoparticle growth orientation and thermodynamic shape. The B reagent besides platinum precursor can lead to different ligand decomposition mechanism when Pt precursors are exposed: oxygen allows more effective ligand combustion compared to water, however, the Pt particles are more oxidized according to XPS studies. We expect this work provides a way for tailoring nanoparticles with desired size, dispersion, exposed surfaces and chemical state etc, which helps controlling and optimizing their performance when applied as catalysts or nanosensors.

Keywords: atomic layer deposition, TEM, XPS, nanoparticles, platinum

(Some figures may appear in colour only in the online journal)

1. Introduction

In recent decades, methods of producing Pt nanocrystals have been of great interests due to their application in many catalytic processes, e.g. Enterkin *et al* showed SrTiO$_3$ nanocuboids supported Platinum nanoparticles are a low temperature hydrocarbon catalyst for automotive applications [1]. Gullon *et al* reported preferentially oriented Pt nanoparticles can be used for methanol and formic acid electrooxidation [2]. Bratelie *et al* demonstrated that the selectivity of benzene

hydrogenation catalyzed by Pt nanocrystals is shape-dependent [3]. Croy *et al* mentioned that decomposition of methanol can be accomplished by Pt nanoparticles supported on nanocrystalline anatase TiO$_2$ [4]. Well-controlled synthesis of these nanocrystals is critical to correlate properties of interest such as size, shape, composition and exposed surfaces to catalytic performance. However, with traditional preparation techniques including impregnation [5], ion-exchange [6–8], and deposition-precipitation [9, 10], the metal nanoparticles usually lack atomic-level control of the catalyst composition and surface structure, yielding relatively large metal clusters with a broad size distribution,

[4] Author to whom any correspondence should be addressed.

J. Phys. D: Appl. Phys. **50** (2017) 415301

C Wang *et al*

extremely low loading and exposed surfaces with undetermined orientation [11–14].

Lately, atomic layer deposition (ALD) has been applied to synthesize both metal [15, 16] and metal oxide [17]catalytic materials. ALD was originally developed for the production of thin film materials in the late 1970s by Suntola *et al* [18, 19]. It relies on self-limiting, sequential binary reactions between gaseous precursor molecules and a substrate in a layer by layer fashion. However, initial stage of metal ALD usually suffers from poor nucleation and the growth initiates as discrete islands on most substrates [20]. By exploiting this merit, ALD can be used as a technique for controllably depositing kinetically stable particles with high dispersions, large surface area and determined surface orientation etc [21, 22]. More advantages of this technique for the synthesis of metal nanoparticles have been discussed extensively [23–25]. The aim of this work is to elucidate how specific ALD variables influence Pt nanoparticle size, density, loading, exposed surface and chemical state. Variables of interest include type of ALD method, reaction temperature, number of cycles, reagents besides metal precursor and substrates. Three ALD methods have been investigated for Pt nanoparticle synthesis: (1) traditional AB-type, (2) ABC-type and (3) static ABC-type ALD. The impact of reaction temperature, performed ALD cycles, type of substrates and precursor identity on particle formation have also been discussed, which play a critical role on the deposition process.

2. Experimental

2.1. Two types of STO-NCs substrates

Two types of STO-NCs were used as substrates for Pt ALD deposition both of which were prepared using hydrothermal synthesis. One type of STO-NCs was synthesized using oleic acid (OA) [26] which yields the surface with SrO termination. However, using acetic acid (AA) [27] during the synthesis results the STO-NCs in TiO_2 rich reconstruction mix with SrO termination [28]. The existing difference in surface termination of these two types of STO-NCs helps facilitating the study of Pt nanoparticle formation on these two different surfaces [28, 29]. In this study we will refer STO-NCs synthesized using OA and AA as STO-NCs (OA) and STO-NCs (AA).

2.2. Platinum ALD

All depositions were accomplished in a viscous flow reaction chamber with a base pressure of 0.3 Torr. An ultrahigh purity (99.999%) nitrogen (N_2) flow of 125 standard cubic centimeters per min (sccm) increases the chamber pressure to 1 Torr during deposition. This reactor was equipped with a (trimethyl)methylcyclopentadienylplatinum (IV) ($MeCpPtMe_3$, Sigma-Aldrich 99%) bubbler, a titanium isopropoxide (TTIP, $Ti(OCH(CH_3)_2)_4$, Sigma-Aldrich, 97%) bubbler, oxygen cylinder (99.99%) and a millipore water doser. During ALD, all necessary precursor bubblers are heated to an appropriate temperature to achieve sufficient vapor pressure, e.g. $MeCpPtMe_3$ 50 °C, TTIP 100 °C and water room temperature.

Traditional ALD is a two-step process usually consists of alternating A/B precursor exposure, with each step separated by N_2 purging, e.g. $MeCpPt(Me)_3$ was used as precursor (A) and oxygen or water was used for precursor (B) which will also be referred to as AB type ALD in this study. During ALD synthesis, a 5 sccm N_2 flow was passed through the bubbler to assist in the transport of $MeCpPtMe_3$ to the reaction chamber, while Reagent B, C was delivered as vapor drop without any carrier flow. The timing sequence is expressed as t_1–t_2–t_3–t_4, where t_1 is the $MeCpPtMe_3$ precursor dose time and t_2 is the purge time, t_3 is the water or oxygen dose time and t_4 is the corresponding purge time. The specific times used here were 300 s–600 s–120 s–600 s. In order to increase Pt nanoparticle loading without changing particle size, the newly developed ABC-type ALD method was also performed. This method consists of three alternating precursors, A–C, which were $MeCpPtMe_3$ (A), TTIP (B) and water (C), respectively [25]. The timing sequence used here was t_1–t_2–t_3–t_4–t_5–t_6, where t_1, t_2 are the time length for the $MeCpPtMe_3$ precursor dose and subsequent purging time; t_3, t_4 are the TTIP dose and the following purging time; t_5, t_6 are the water dose and final purging time, which were 300 s–600 s–60 s–600 s–120 s–600 s in this experiment.

For Pt deposition with these precursors, static ABC-type ALD is similar to ABC with related dosing sequence. The major difference between these two is that regular ABC-type has a continuous 125 sccm N_2 flow through the reactor and the process pressure variation is <0.2 Torr during the entire operation. However, for static ABC-type the exhaust valve is closed during Pt precursor exposure with only a 5 sccm N_2 flow used for Pt precursor delivering. As a result, ALD reactor pressure drifts from base pressure ~0.34 Torr to 4.1 Torr at end of Pt precursor exposure. Comparing to AB-type and ABC-type ALD, sample prepared using static ABC-type ALD has longer Pt precursor exposure time and such influence will be discussed later.

2.3. Characterization

The size, density and morphology of Pt nanoparticles were determined with high-resolution transmission electron microscopy (HRTEM) and high angle annular dark field (HAADF) using JOEL2100 operated at 200 kV. All TEM samples were prepared by dripping some ethanol dispersed as-synthesized Pt/STO-NCs onto the surface of a lacey carbon film supported on a copper grid. The Pt weight loading was determined using inductively coupled plasma atomic emission spectroscopy (ICP-AES) (Varian VISTA ICP-AES), which was prepared by dissolving 5 mg of Pt/STO-NCs in a mixture of 1 ml of nitric acid with 3 ml of hydrochloric acid for 48 h to form a clear light yellow solution. Chemical composition and state of the different elements in Pt/STO-NCs were analyzed using x-ray photoelectron spectroscopy (XPS) (ESCALAB 250Xi, Thermo Scientific) with a monochromatic Al Ka (1486.6 eV) anode. The experimental resolution was better than 0.1 eV and a low energy electron flood gun was used during data acquisition to reduce binding energy shifts caused by charging. The XPS sample is prepared by
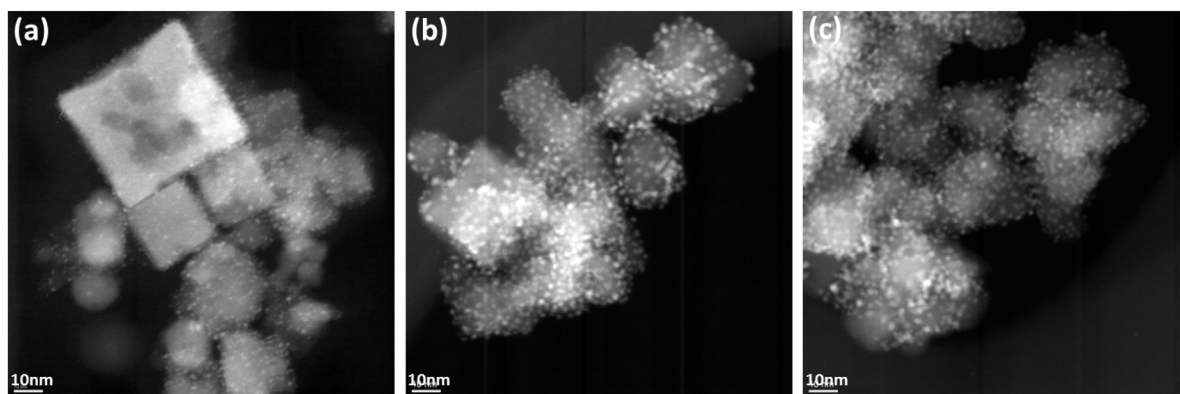
J. Phys. D: Appl. Phys. 50 (2017) 415301

C Wang *et al*

Figure 1. HAADF images of Pt/STO-NCs(OA) synthesized under reaction temperatures of (a) 200 °C (b)250 °C (c) 300 °C.

punching Pt/STO-NCs powder onto a copper tape to form a ~1 mm thick wafer.

3. Results and discussion

3.1. Temperature dependence of Pt ALD synthesis

The temperature dependence of the Pt ALD process is studied by depositing a single cycle of $MeCpPtMe_3/H_2O$ on STO-NCs (OA) within the temperature window of 125 °C–300 °C using different ALD methods. Figure 1 shows three HAADF images of Pt/STO-NCs (OA) deposited at 200 °C, 250 °C and 300 °C using AB-type ALD, suggesting Pt nanoparticles were uniformly dispersed on STO-NCs (OA) with a narrow size distribution of ~1–2 nm for studied temperatures range. The reaction temperature affects the combustion of precursor fragments at the start of $MeCpPt(Me)_3$ adsorption which will alter the net Pt deposition [30]. As reported by Mackus *et al*, activation of the adsorption of the $MeCpPt(Me)_3$ precursor is not the limiting factor during the reaction [31]. The precursor absorbs onto the substrate through ligand exchange between surface hydroxyl groups and methyl ligands of $MeCpPt(Me)_3$. Higher reaction temperatures lead to a higher percentage of decomposed and combusted ligands, resulting in more net Pt single atoms on the STO-NC surface. These single atoms are not energetically stable and continuous surface nucleation process quickly takes place. As the nucleation process will consume Pt atoms around the newly formed Pt nucleus which makes the Pt concentration below the minimum requirement for nucleation, thus nucleation stops whereas growth continues. The growth process after nucleation is denoted by diffusion of Pt atoms that originate relatively far from the nucleus to the nucleus surface. It has been mentioned by Zhou *et al*, the diffusion of Pt atoms is sufficiently activated at ALD reaction temperature to allow for Pt atom transport to larger clusters [32]. We expect the final Pt particle size after one complete cycle will increase with increasing ALD reaction temperature due to increased net Pt deposition [30]. As figure 2 corroborated, particle size increases with ALD reaction temperature in the investigated temperature window.

Platinum particle density (number of Pt particles per unit area) was measured by counting the number of particles in a selected area as illustrated in figure 3(a), the measured
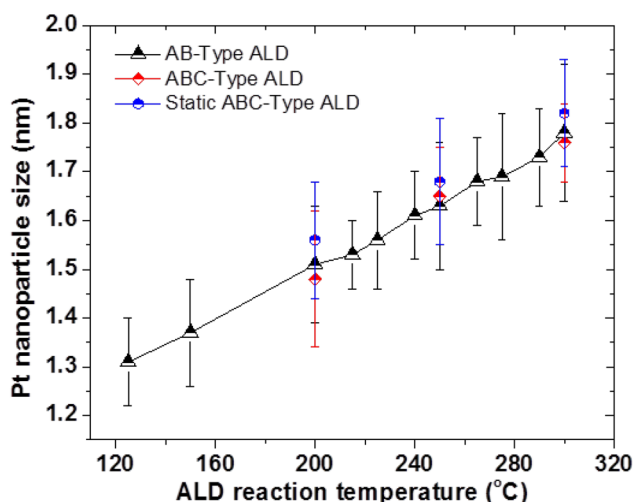

Figure 2. Pt particle size of Pt/STO-NCs (OA) prepared using different types of ALD method as a function of ALD reaction temperature after 1 cycle deposition. Each present data is an average of ~80 measurements. The error bar is standard deviation of all measurements.

results (averaged result of ~20 measurement) were plotted as a function of temperature in figure 3(b). During a single measurement of nucleation density, sample tilting effect is avoided by selectively measuring nanocuboids aligned along the $\langle 100 \rangle$ zone axis in a HAADF image. Measured nucleation density has been divided by 2 considering Pt particles were uniformly deposited on both top and bottom surfaces. As shown in figure 3(b), particle density also increases with reaction temperature which is strongly determined by nucleation density after Pt precursor deposition. As reaction temperature increased, more precursor ligand fragments are eliminated and steric hindrance effects are alleviated which allows more $MeCpPtMe_3$ molecules to be adsorbed, resulting in more Pt atoms on STO surface [33]. Nucleation rate will increase when more Pt atoms are presented on the surface which leads to final nucleation density increase. As indicated by figure 3(b), particle density increased ~13% over the investigated temperature window (125 °C–300 °C).

As Pt particle size and nucleation density vary with ALD reaction temperature, Pt loading which is determined by these two factors will also expected to be temperature dependent. As indicated by ICP-AES analysis shown in figure 4, Pt loading
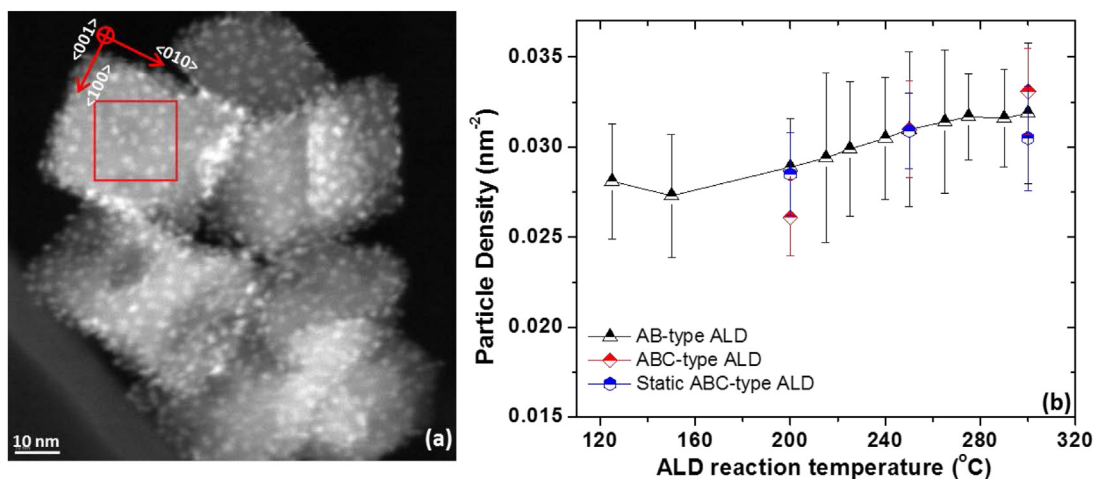
Figure 3. (a) Diagram shows definition of particle density based on a HAADF image of Pt/STO-NCs (OA) synthesized with 1 cycle AB type ALD at 300 °C. (b) Pt particle density prepared with 1 cycle of different ALD methods as a function of ALD reaction temperature. The error bar here is standard deviation of ~20 measurements.

also increase with reaction temperature. When the reaction temperature was low as 125 °C, a relatively low loading of 1.94% (27.7 ng cm^{-2}) was observed after a single cycle ALD. For temperatures above 150 °C, Pt nanoparticle loading was found to be roughly linearly increasing increase with reaction temperature up to 275 °C. A similar behavior was previously reported by Mackus *et al* for Pt ALD conducted in a temperature range between 150 and 450 °C [34]. Temperature above 300 °C is not further investigated, as it is beyond our ALD safety operation limit.

Additional HAADF images of Pt/STO-NCs (OA) synthesized using ABC-type and static ABC-type ALD suggest that the temperature dependences of particle size and nucleation density are similar to AB-type ALD for a single cycle of deposition, figures 2 and 3. However, nanoparticles acquired by static ABC-type ALD are found to be slightly larger than those formed with the other two methods at the same ALD reaction temperature. This is likely due to more Pt precursor exposure in a close pump environment yields more net Pt deposition.

3.2. Dependence of Pt nanoparticle size and density on number of ALD cycles and ALD methods

In following, influence of number of ALD cycles on obtained Pt nanoparticle size, nucleation density and weight loading are discussed. Pt/STO-NCs (OA) samples studied here were prepared using different ALD methods at 200 °C and 300 °C with single and multiple cycle deposition. The effect of temperature, number of cycles and type of ALD methods were investigated and the results were summarized in table 1. Pt nanoparticle size synthesized with 1, 5 cycles of traditional AB-type ALD were 1.51 nm, 1.80 nm (200 °C) and 1.78 nm, 2.25 nm (300 °C) in diameter respectively implying that Pt particles grow with increasing number of ALD cycles. Increase in size of Pt particles per cycles is determined by net Pt deposition during that cycle according to our previous work [30]. Once a Pt atom is deposited during a continuous cycle, it will diffuse, attach to a previously formed nanoparticle surface and contributes to particle growth [32]. Meanwhile as shown in
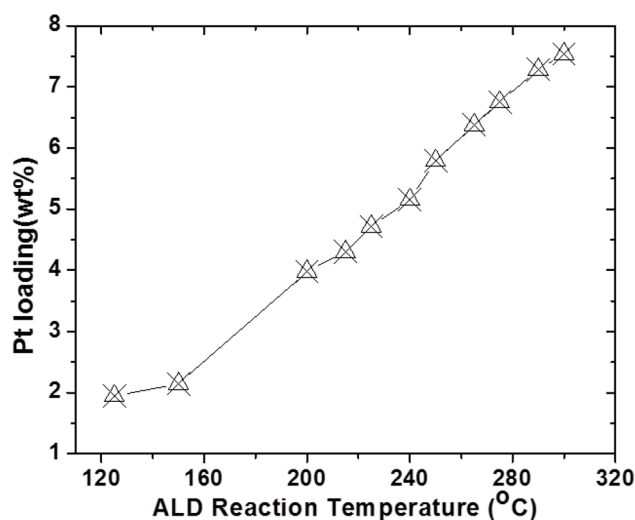

Figure 4. ICP-AES measured Pt weight loading of Pt/STO-NCs (OA) as a function of ALD reaction temperature.

figure 5, the nucleation density was negligibly increased with number of ALD cycles, indicating that no new nucleation and coalescence processes take place during Pt precursor exposure in each new ALD cycle.

However, for Pt nanoparticles prepared using ABC-type and static ABC-type ALD, HAADF images show the cycle dependence is different. Increase of particle density occurs instead of particle size growth comparing to traditional AB-type ALD. As detailed by Lu *et al*, the increase in Pt nucleation density of continuous cycles is caused by the creation of new nucleation sites on the STO-NCs surface during the BC portion of the ABC-type ALD process (or static ABC) before the next Pt precursor dose [25]. Platinum precursor exposed to freshly regenerated supporting surface will mainly yield new nucleation similar to the 1st cycle. As a result, the number of particles per unit area increases which is indicated by increased nucleation density and slightly increased particle size in table 1. In the case of static ABC-type ALD, the reactions taking place during each cycle are a combination of traditional AB-type and ABC-type ALD. Similar to ABC-type

J. Phys. D: Appl. Phys. **50** (2017) 415301

C Wang *et al*

Table 1. Dependence of Pt nanoparticles size and density of Pt/STO-NCs (OA) on number of ALD cycles and type of ALD methods at 200 °C and 300 °C.

	200 °C					
	AB-type ALD		ABC-type ALD		Static ABC-type ALD	
# of cycles	Size (nm)	Particle density (nm^{-2})	Size (nm)	Particle density (nm^{-2})	Size (nm)	Particle density (nm^{-2})
1	1.51	0.0281	1.48	0.0261	1.56	0.0285
4	—	—	1.51	0.0381	1.63	0.0393
5	1.80	0.0297	—	—	—	—
	300 °C					
1	1.78	0.0319	1.76	0.0331	1.82	0.0305
4	—	—	1.83	0.0392	1.91	0.0397
5	2.25	0.0297	—	—	—	—

ALD, a fresh surface with surface hydroxyl groups is generated prior to the Pt precursor dose which leads to new Pt particle growth. However during the dose the reaction chamber is isolated from pumping, particle growth will take place besides nucleation due to more net Pt deposition. As a result both particle size and nucleation density will increase with number of cycles increase.

Cycle dependence of three ALD methods at elevated reaction temperature of 300 °C is comparable to the dependence at 200 °C. However, impacts of reaction temperature on the synthesis need to be considered. As discussed in section 3.1, ALD accomplished at higher reaction temperature will yield larger particles and slightly higher nucleation density. Dependence of number of cycles for the three ALD methods at higher reaction temperature was also summarized in table 1, which indicates cycle dependence of particle size and nucleation density of Pt nanoparticles prepared at 300 °C are comparable to these prepared at 200 °C but with larger particle size and higher density.

3.3. Influence of STO-NC substrates on the structure of formed Pt nanoparticle

We focus predominantly here on discussing the influence of the substrate to Pt nanoparticles synthesis. Two types of STO-NCs were used as supporting substrates in this study, both of which were characterized to be with sharp corners, a narrow size distribution, and predominant exposure of the (100) surface. Due to different used precursor and synthesis condition, detail HRTEM studies reveal STO-NCs (OA) with SrO termination while STO-NCs (AA) with TiO$_2$-rich reconstruction mixed with SrO termination [26, 27]. The structure and growth orientation of Pt nanoparticles on these two types of STO-NCs are different due to difference in surface terminations [35, 36]. As reported by Enterkin *et al*, Pt nanoparticle deposited on TiO$_2$ rich STO-NCs (AA) will only grows in direction of ⟨100⟩ [35]. However, as shown in figure 6, Pt nanoparticles deposited on STO-NCs (OA) grow in both ⟨100⟩ and ⟨111⟩ directions. The determination of Pt growth orientation on surface termination of SC-STO substrates can be understood in terms of an associated balance of chemical bond strength and particle surface energy across the interface [36]. In the case of Pt on TiO$_2$-terminated STO synthesized
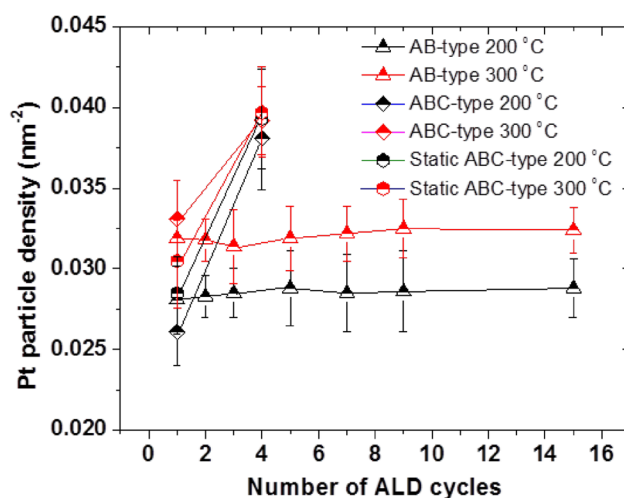

Figure 5. Pt particle density of Pt/STO-NCs (OA) as a function of number of ALD cycle under two different ALD reaction temperatures of 200 °C and 300 °C. The error bar is standard deviation of ~20 measurements.

with AA, epitaxial orientations minimize this as a higher degree of chemical bonding exists when Pt grows in ⟨100⟩. On the SrO terminated surface, as a mismatch of lattice fringe exists between the Pt and SrO terminated surface, bonds between Pt and STO surface are weaker which leads to growth of Pt in both the ⟨100⟩ and ⟨111⟩ directions. The shape of Pt particles is also determined by substrates and can be predicted by Winterbottom construction as shown in figure 6 [37]. The Winterbottom reconstruction is modified from Wulff construction [38] which describes how the interface free energy will determine the degree of truncation of a free particle when it is formed on a substrate. The truncated location is determined by the difference between the interfacial energy and the substrate free energy which varies due to surface termination [35]. With different termination present, a changing of growth orientation and truncation of the Wulff shape will take place which yield Pt particles with apparently different shape.

3.4. Role of reagent in ALD process

Pt ALD is often performed using oxygen at 300 °C to decompose the Pt precursor [31, 39, 40]. Other reagents have also been investigated for the synthesis, the purpose of which is
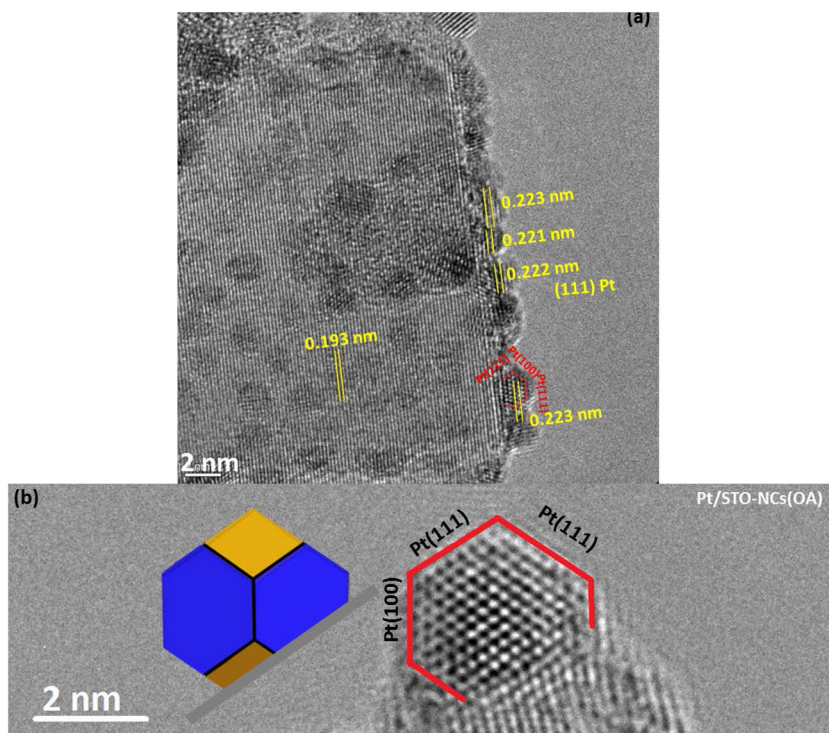
Figure 6. (a) HREM image of Pt on the (1 0 0) face of STO-NCs (OA) with SrO termination. The Pt nanoparticle can be differentiated from the STO substrate by measuring the lattice fringes. (b) Winterbottom shape for platinum nanoparticle is overlaid upon Pt nanoparticle in red.

either to reduce, oxidize or provide new nucleation sites on the supporting material for the next metal precursor dosing [33]. Water and oxygen are found to be effectively helping the deposition of Pt particles in this work according to ICP-AES and XPS studies. ICP-AES analysis suggests a Pt weight loading of 8.9% (water) and 14.8% (oxygen) for 8 cycles ALD synthesis at 250 °C on STO-NCs (AA), which indicates that oxygen are more effectively for Pt deposition than water. XPS analysis also shows a similar phenomenon for Pt deposited on STO-NCs (AA). As shown in figure 7, a higher I(Pt 4f)/I(Ti 2p) peak ratio (after adjustment with the appropriate Scofield factor), except for the 1st cycle, was found for Pt/STO-NCs (AA) prepared using oxygen, as opposed to water under the same synthesis conditions. Figure 8 shows XPS Pt 4f peaks of as-synthesized Pt/STO-NCs (AA) using water and oxygen as the B reagent (8 cycles at 250 °C) which demonstrates obvious change in chemical state. For either synthesis, XPS Pt 4f peaks shows coexistence of three components Pt (0), Pt (II) and Pt (IV). Pt(0) and Pt(II) + Pt(IV) percentage according to XPS peak fitting, calculated as I(Pt(0))/(I(Pt(0) + I(Pt(II)) + I(Pt(IV))) and I(Pt(II) + Pt(IV))/(I(Pt(0) + I(Pt(II)) + I(Pt(IV))), was plotted as a function of the number of ALD cycles in figure 9, which indicates that Pt ALD using oxygen yields more oxidized Pt than water after the same number of ALD cycles. Pt(II) and Pt(IV) shoulder presents in Pt 4f XPS peaks are contributed by two sources: PtO$_x$ monolayer formed on the Pt nanoparticle surface and Pt–O bonds presented at the interface between the metal and oxide support, as Pt ALD usually start with ligand exchange of Pt precursor and surface hydroxyl groups [36, 41]. A decrease of Pt(II) + Pt(IV) to Pt(0) ratio is expected as surface to volume ratio decreases with particle size.
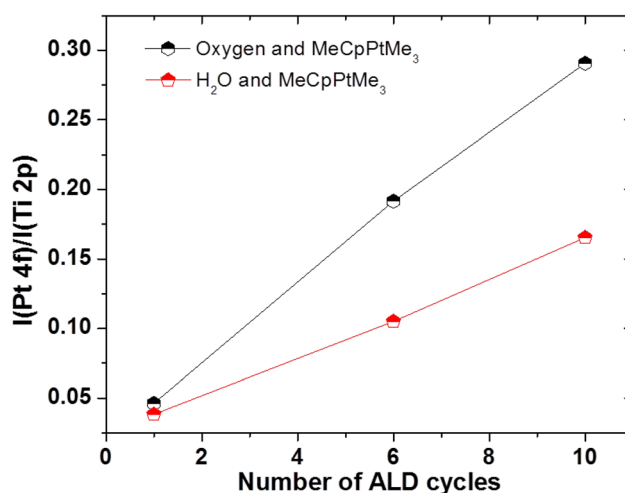

Figure 7. XPS Pt 4f/Ti 2p ratio of Pt/STO-NCs (AA) deposited using oxygen and water as a function of deposition cycles.

For Pt ALD using oxygen as a B reagent, the amount of adsorbed oxygen that resides at the STO-NC surface after the O$_2$ exposure is important which will affect the nature of the reaction during the MeCpPtMe$_3$ pulse and the amount of adsorbing precursor molecules. The present oxygen atoms lead to combustion of ligands during MeCpPtMe$_3$ exposure. If ligands are eliminated before next precursor exposure, steric hindrance effects are alleviated and more MeCpPtMe$_3$ molecules can adsorb, resulting in a higher growth rate. Surface science results suggest that combustion of ligands takes place above ~300 K (27 °C) when oxygen and hydrocarbons are both present at the surface which is easily met for typical Pt
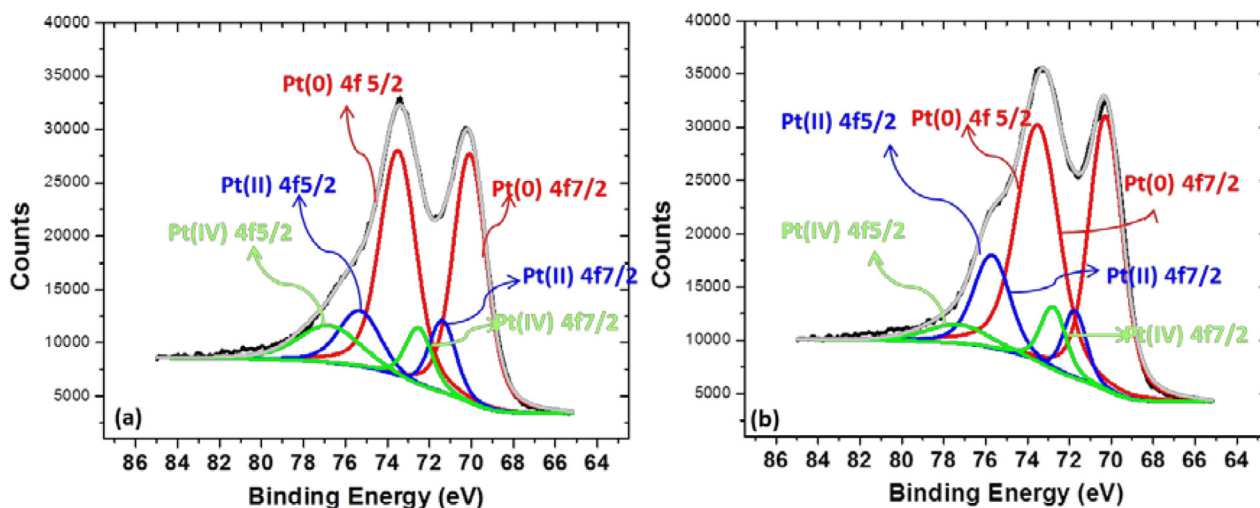
Figure 8. XPS Pt 4f spectroscopy of Pt/STO-NCs (AA) deposited with 8 cycles AB type ALD at 250 °C (a) oxygen (b) water.
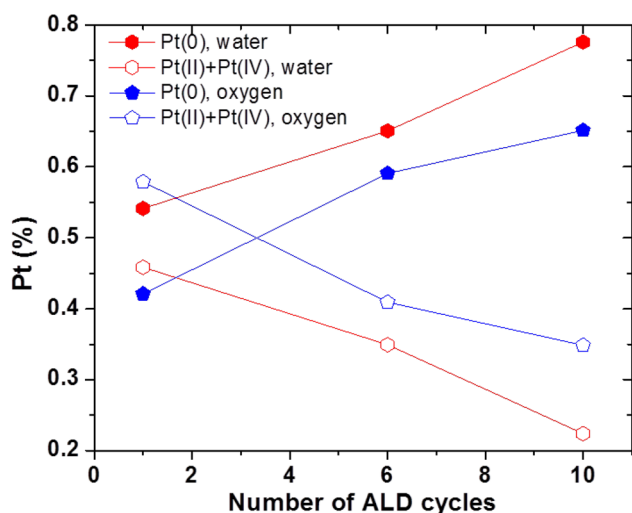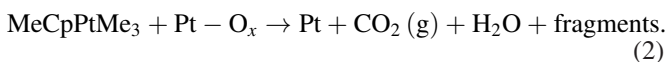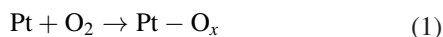

Figure 9. Pt(0) and Pt(II) + Pt(IV) percentage of Pt/STO-NCs (AA) deposited using water and oxygen as a function of number of ALD cycles.

Figure 10. XPS I(C 1s)/I(Sr 3p) ratio of Pt/STO-NCs (AA) prepared using water and oxygen as B reagent.

ALD reaction conditions (125 °C–300 °C) in this work [42]. As reported by Hiratani *et al*, the reaction mechanism of Pt ALD using oxygen as a B reagent relies on autocatalytic oxidation of MeCpPtMe$_3$ [43],

$$Pt + O_2 \rightarrow Pt - O_x \tag{1}$$

$$MeCpPtMe_3 + Pt - O_x \rightarrow Pt + CO_2\,(g) + H_2O + \text{fragments.} \tag{2}$$

In equation (1), Pt–O$_x$ represents molecular O$_2$ or dissociated O atoms on the Pt surface. The activation of the oxygen by dissociation into atomic oxygen on the Pt surface should not be difficult as oxygen can easily be dissociated at temperatures >120 K [44]. Formed Pt–O$_x$ will react with adsorbed MeCpPtMe$_3$ precursors in an oxidative decomposition reaction (equation (2)), resulting in CO$_2$ and H$_2$O reaction products, and possibly some hydrocarbon fragments.

Several studies have suggested that surface hydroxyl groups are involved in the reaction of Pt ALD [45–47]. Thus water can also be used as second reagent for Pt ALD process in order to regenerate hydroxyl groups on the oxide surface.
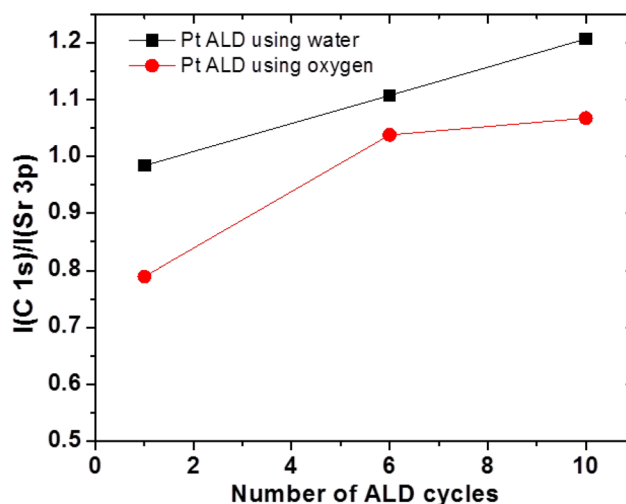
As pointed out by Christensen *et al*, the proposed mechanism for water based Pt ALD begins with ligand exchange between the methyl groups of the MeCpPtMe$_3$ molecule and hydroxyl groups [33]. The elimination of ligands is accomplished through thermal decomposition here instead of oxidative decomposition happened when oxygen is used as B reagent. However, carbon removal through thermal decomposition is less efficient than oxidation removal when oxygen is used. As a result, more carbonaceous layers will present for Pt/STO-NCs prepared using water. As supported by XPS analysis of C1s level of as-synthesized Pt/STO-NCs (AA) prepared using water and oxygen (figure 10), C 1s/Sr 3p of Pt/STO-NCs (AA) prepared with water shows higher ratio than oxygen with all other synthesis conditions held to be same. While water is used for Pt synthesis, hydroxyl groups dissociate from water may interact with Pt nanoparticles and have a tendency to combine to produce a water molecule and a O^{2-} anion through Bronsted acid/base reactions (OH$^-$ + OH$^-$ → O^{2-} + H$_2$O(g)) [48]. O^{2-} generated here may assist ligand oxidative combustion. However, this effect is very weak compared to oxygen is directly used as the oxidant.

J. Phys. D: Appl. Phys. **50** (2017) 415301

C Wang *et al*

4. Conclusion

The influences of different parameters, e.g. reaction temperature, number of cycles, substrate, reagents and type of ALD method, on the synthesis of Pt nanoparticles have been investigated individually in this work. Particle size, density and loading vary with reaction temperature, number of cycles and type of ALD methods. Pt growth orientation and shape can be changed by using different types of substrates. Changing the oxidizing/protonolytic reagent can leads to different chemical states and compositions of synthesized Pt particles. This work also opens a way for better understanding of metal nanoparticle synthesis using ALD. A precise control of size, density, growth orientation and exposed surface etc can be accomplished by tuning the different parameter discussed above. We expect this work will help tailoring performance when these particles are used for catalytic or nanosensing purposes, as their performance are heavily dependent on these properties.

Acknowledgments

References

[1] Enterkin J A *et al* 2011 Propane oxidation over Pt/SrTiO₃ nanocuboids *ACS Catal.* **1** 629–35

[2] Solla-Gullon J *et al* 2008 Shape-dependent electrocatalysis: methanol and formic acid electrooxidation on preferentially oriented Pt nanoparticles *Phys. Chem. Chem. Phys.* **10** 3689–98

[3] Bratlie K M *et al* 2007 Platinum nanoparticle shape effects on benzene hydrogenation selectivity *Nano Lett.* **7** 3097–101

[4] Croy J R *et al* 2007 Size dependent study of MeOH decomposition over size-selected pt nanoparticles synthesized via micelle encapsulation *Catal. Lett.* **118** 1–7

[5] Lu C Y *et al* 2009 The comparison between the polyol process and the impregnation method for the preparation of CNT-supported nanoscale Cu catalyst *Chem. Eng. J.* **145** 461–7

[6] Bonivardi A L, Baltanas M A and Chiavassa D L 1993 Structural support effects in the systematic preparation of Pd/SiO₂ catalyst for methanol synthesis by ion-exchange techniques *Stud. Surf. Sci. Catalysis* **75** 1801–4

[7] Fujitani T and Echigoya E 1991 Preparation of highly-active palladium catalyst supported on silica by ion-exchange method *Nippon Kagaku Kaishi* **1991** 1475–81

[8] Ohman L O *et al* 2002 Catalyst preparation through ion-exchange of zeolite Cu-, Ni-, Pd-, CuNi- and CuPd-ZSM-5 *Mater. Chem. Phys.* **73** 263–7

[9] Murzin D Y *et al* 2011 Thermodynamic analysis of the cluster size evolution in catalyst preparation by deposition-precipitation *React. Kinetics Mech. Catal.* **104** 259–66

[10] Salim V M M *et al* 1995 Preparation of highly loaded nickel/silica catalysts by a deposition-precipitation method. Effect of the aging time on the reducibility of nickel and on the textural properties of the catalyst *Stud. Surf. Sci. Catalysis* **91** 1017–26

[11] Stair P C 2008 Advanced synthesis for advancing heterogeneous catalysis *J. Chem. Phys.* **128** 182507

[12] Lopez T *et al* 1992 Spectroscopic characterization and catalytic properties of sol-gel Pd/SiO₂ catalysts *J. Catal.* **138** 463–73

[13] Xie Y *et al* 2009 *In situ* controllable loading of ultrafine noble metal particles on titania *J. Am. Chem. Soc.* **131** 6648

[14] Okamoto K *et al* 2005 Formation of nanoarchitectures including subnanometer palladium clusters and their use as highly active catalysts *J. Am. Chem. Soc.* **127** 2125–35

[15] Lei Y *et al* 2012 Synthesis of Pt–Pd core–shell nanostructures by atomic layer deposition: application in propane oxidative dehydrogenation to propylene *Chem. Mater.* **24** 3525–33

[16] Christensen S T *et al* 2010 Supported Ru–Pt bimetallic nanoparticle catalysts prepared by atomic layer deposition *Nano Lett.* **10** 3047–51

[17] Lee M *et al* 2010 Fabrication and applications of metal-oxide nano-tubes *JOM* **62** 44–9

[18] Suntola T A 1977 *US Patent* 4,058,430

[19] Suntola T and Hyvarinen J 1985 Atomic layer epitaxy *Annu. Rev. Mater. Sci.* **15** 177–95

[20] Elam J W *et al* 2007 Nucleation and growth of noble metals on oxide surfaces using atomic layer deposition *ECS Trans.* **3** 271–8

[21] Liu C *et al* 2009 Atomic layer deposition of platinum nanoparticles on carbon nanotubes for application in proton-exchange membrane fuel cells *Small* **5** 1535–8

[22] King J S *et al* 2008 Ultralow loading Pt nanocatalysts prepared by atomic layer deposition on carbon aerogels *Nano Lett.* **8** 2405–9

[23] Elam J W *et al* 2006 Atomic layer deposition of palladium films on Al₂O₃ surfaces *Thin Solid Films* **515** 1664–73

[24] Lu J L and Stair P C 2010 Nano/subnanometer Pd nanoparticles on oxide supports synthesized by AB-type and low-temperature ABC-type atomic layer deposition: growth and morphology *Langmuir* **26** 16486–95

[25] Lu J L and Stair P C 2010 Low-temperature ABC-type atomic layer deposition: synthesis of highly uniform ultrafine supported metal nanoparticles *Angew. Chem., Int. Ed. Engl.* **49** 2547–51

[26] Hu L H *et al* 2013 SrTiO₃ nanocuboids from a Lamellar microemulsion *Chem. Mater.* **25** 378–84

[27] Rabuffetti F A *et al* 2008 Synthesis-dependent first-order Raman scattering in SrTiO₃ nanocubes at room temperature *Chem. Mater.* **20** 5628–35

[28] Lin Y Y *et al* 2013 Synthesis-dependent atomic surface structures of oxide nanoparticles *Phys. Rev. Lett.* **111** 156101

[29] Deak D S 2007 Strontium titanate surfaces *Mater. Sci. Technol.* **23** 630

[30] Wang C, Hu L, Poeppelmeier K, Stair P C and Marks L D 2017 Nucleation and growth processes of atomic layer deposition platinum nanoparticles on strontium titanate nanocuboids *Nanotechnology* **28** 185704

[31] Mackus A J M *et al* 2013 Influence of oxygen exposure on the nucleation of platinum atomic layer deposition: consequences for film growth, nanopatterning, and nanoparticle synthesis *Chem. Mater.* **25** 1905–11

[32] Zhou Y *et al* 2012 Growth of Pt particles on the anatase TiO₂ (101) surface *J. Phys. Chem.* C **116** 12114–23

[33] Setthapun W *et al* 2010 Genesis and evolution of surface species during Pt atomic layer deposition on oxide supports characterized by *in situ* XAFS analysis and water-gas shift reaction *J. Phys. Chem.* C **114** 9758–71

[34] Mackus A J M *et al* 2012 Catalytic combustion and dehydrogenation reactions during atomic layer deposition of platinum *Chem. Mater.* **24** 1752–61

[35] Enterkin J A, Poeppelmeier K R and Marks L D 2011
　　　Oriented catalytic platinum nanoparticles on high surface
　　　area strontium titanate nanocuboids *Nano Lett.* **11** 3510

[36] Polli A D *et al* 2000 Growth of platinum on TiO_2- and SrO-
　　　terminated $SrTiO_3(1\,0\,0)$ *Surf. Sci.* **448** 279–89

[37] WinterboW L 1967 Equilibrium shape of a small particle in
　　　contact with a foreign substrate *Acta Metall.* **15** 303

[38] Wulff G 1901 On the question of speed of growth and
　　　dissolution of crystal surfaces *Z. Krystallogr. Miner.*
　　　1901 449–530

[39] Aaltonen T *et al* 2003 Reaction mechanism studies on atomic
　　　layer deposition of ruthenium and platinum *Electrochem.
　　　Solid State Lett.* **6** C130–3

[40] Aaltonen T *et al* 2003 Atomic layer deposition of platinum
　　　thin films *Chem. Mater.* **15** 1924–8

[41] Asthagiri A and Sholl D S 2002 First principles study of
　　　Pt adhesion and growth on SrO- and TiO_2-terminated
　　　$SrTiO_3(1\,0\,0)$ *J. Chem. Phys.* **116** 9914–25

[42] Marsh A L and Gland J L 2003 Mechanisms of deep benzene
　　　oxidation on the Pt(1 1 1) surface using temperature-
　　　programmed reaction methods *Surf. Sci.* **536** 145–54

[43] Hiratani M *et al* 2001 Platinum film growth by chemical vapor
　　　deposition based on autocatalytic oxidative decomposition
　　　J. Electrochem. Soc. **148** C524–7

[44] Gland J L, Sexton B A and Fisher G B 1980 Oxygen
　　　interactions with the Pt(1 1 1) surface *Surf. Sci.* **95** 587–602

[45] Elliott S D 2010 Mechanism, products, and growth rate of
　　　atomic layer deposition of noble metals *Langmuir* **26** 13020

[46] Kessels W M M *et al* 2009 Surface reactions during atomic
　　　layer deposition of Pt derived from gas phase infrared
　　　spectroscopy *Appl. Phys. Lett.* **95** 013114

[47] Christensen S T and Elam J W 2010 Atomic layer deposition
　　　of Ir–Pt alloy films *Chem. Mater.* **22** 2517–25

[48] Eisert F, Elg A P and Rosen A 1995 Adsorption of oxygen and
　　　hydrogen on Pt(1 1 1) studied with 2nd-harmonic generation
　　　Appl. Phys. A **60** 209–15